



Originally published as:

Rodríguez-Zuluaga, J., Stolle, C., Yamazaki, Y., Lühr, H., Park, J., Scherliess, L., Chau, J. (2019): On the balance between plasma and magnetic pressure across equatorial plasma depletions. - *Journal of Geophysical Research*, 124, 7, pp. 5936—5944.

DOI: <http://doi.org/10.1029/2019JA026700>

## JGR Space Physics

## RESEARCH ARTICLE

10.1029/2019JA026700

## Special Section:

Equatorial Aeronomy: New Results From the 15th International Symposium on Equatorial Aeronomy (ISEA-15) and Beyond

## Key Points:

- First observational evidence of high plasma pressure in depleted density regions in the ionosphere
- High-pressure plasma depletions are suggested to exhibit temperatures at least twice the background
- Particle precipitation is a likely heating source due to the longitudinal distribution of the events

## Correspondence to:

J. Rodríguez-Zuluaga,  
juanrz@gfz-potsdam.de

## Citation:

Rodríguez-Zuluaga, J., Stolle, C., Yamazaki, Y., Lühr, H., Park, J., Scherliess, L., & Chau, J. L. (2019). On the balance between plasma and magnetic pressure across equatorial plasma depletions. *Journal of Geophysical Research: Space Physics*, 124, 5936–5944. <https://doi.org/10.1029/2019JA026700>





Received 6 MAR 2019

Accepted 10 JUN 2019

Accepted article online 25 JUN 2019

Published online 10 JUL 2019

## On the Balance Between Plasma and Magnetic Pressure Across Equatorial Plasma Depletions

J. Rodríguez-Zuluaga<sup>1,2</sup> , C. Stolle<sup>1,2</sup> , Y. Yamazaki<sup>1</sup> , H. Lühr<sup>1</sup>, J. Park<sup>3</sup> , L. Scherliess<sup>4</sup> , and J. L. Chau<sup>5</sup> 

<sup>1</sup>GFZ German Research Centre for Geosciences, Potsdam, Germany, <sup>2</sup>Faculty of Science, University of Potsdam, Potsdam, Germany, <sup>3</sup>Korea Astronomy and Space Science Institute, Daejeon, South Korea, <sup>4</sup>Center for Atmospheric and Space Sciences, Utah State University, Logan, UT, USA, <sup>5</sup>Leibniz Institute of Atmospheric Physics, Kühlungsborn, Germany

**Abstract** In magnetized plasmas such as the ionosphere, electric currents develop in regions of strong density gradients to balance the resulting plasma pressure gradients. These currents, usually known as diamagnetic currents decrease the magnetic pressure where the plasma pressure increases, and vice versa. In the low-latitude ionosphere, equatorial plasma depletions (EPDs) are well known for their steep plasma density gradients and adverse effect on radio wave propagation. In this paper, we use continuous measurements of the magnetic field and electron density from the European Space Agency's Swarm constellation mission to assess the balance between plasma and magnetic pressure across large-scale EPDs. The analysis is based on the magnetic fluctuations related to diamagnetic currents flowing at the edges of EPDs. This study shows that most of the EPDs detected by Swarm present a decrease of the plasma pressure relative to the ambient plasma. However, EPDs with high plasma pressure are also identified mainly in the vicinity of the South Atlantic magnetic anomaly. From the electron density measurements, we deduce that such an increase in plasma pressure within EPDs might be possible by temperatures inside the EPD as high as twice the temperature of the ambient plasma. Due to the distinct location of the high-pressure EPDs, we suggest that a possible heating mechanism might be due to precipitation of particle from the radiation belts. This finding corresponds to the first observational evidence of plasma pressure enhancements in regions of depleted plasma density in the ionosphere.

## 1. Introduction

In the Earth's low-latitude ionosphere, large-scale electric currents develop during daytime at the *E* and *F* regions through dynamo processes (e.g., Forbes & Garrett, 1979; Rishbeth, 1971). Different than these currents, other currents do not depend on conductivity but upon the interaction of the plasma with the Earth's gravitational and magnetic fields. This characteristic makes currents such as those driven by gravity and by plasma pressure gradients relevant in the nighttime ionosphere (e.g., Alken et al., 2017). The latter, also known as diamagnetic currents ( $\mathbf{j}_d$ ), are essential to understanding the balance between magnetic and plasma pressure. Although these currents have not been extensively studied, the known theoretical and experimental evidence provides valuable information. Lühr et al. (2003) reported the first magnetic field observations related to  $\mathbf{j}_d$  at the equatorial ionospheric anomaly. The equatorial ionospheric anomaly presents significant meridional gradients of plasma pressure due to its regular plasma density enhancements at 10° to 15° south and north to the dip equator. The authors use magnetic field measurements gathered by the CHAMP satellite to validate the expected magnetic effect associated with  $\mathbf{j}_d$ . Further studies have shown evidence that suggests there is a good balance between magnetic and plasma pressures (e.g., Park et al., 2008; Stolle et al., 2006), especially when the neutral gas is taken into account (e.g., Park et al., 2010). In particular, Stolle et al. (2006) analyze magnetic field fluctuations associated with equatorial plasma depletions (EPDs) and their global distribution by using CHAMP data. In their study, the authors present distinct magnetic fluctuations related to  $\mathbf{j}_d$  at EPDs. In the absence of high-resolution electron density measurements, they use such magnetic signatures to assess the global occurrence rate of EPDs, finding good agreement with previous studies based on plasma density measurements. By using numerical simulations, additional studies have also obtained magnetic field fluctuations related to  $\mathbf{j}_d$  at EPDs with magnitudes similar to those detected by magnetometers on board satellites (e.g., Aveiro et al., 2011; Dao et al., 2013; Yokoyama & Stolle, 2017). The

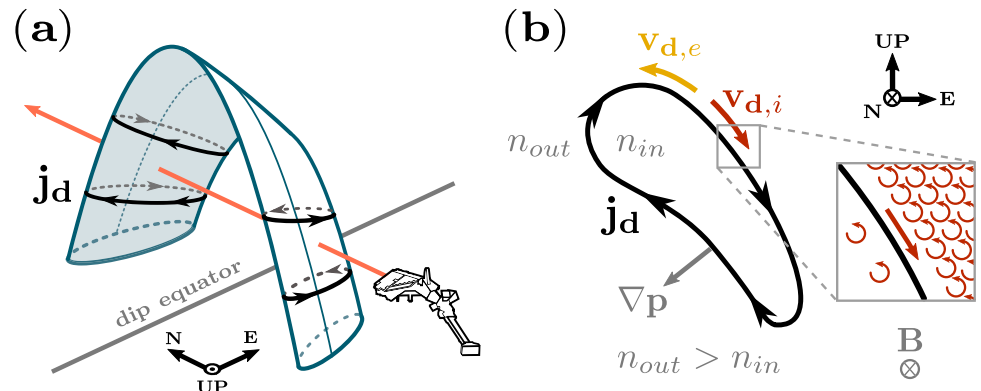


**Figure 1.** (a) Description of a wedge-like EPD, its associated diamagnetic current ( $\mathbf{j}_d$ ), and the path of a Swarm satellite going through the EPD. (b) A zonal cross section at the dip equator of the EPD in (a). It shows the diamagnetic drifts of both ions and electrons ( $\mathbf{V}_{d,i}$ ,  $\mathbf{V}_{d,e}$ ), the plasma pressure gradient ( $\nabla p$ ), and the diamagnetic current ( $\mathbf{j}_d$ ). The box to the right is a zoom in to the ions gyrating in the magnetic field at the edge of the EPD. EPD = equatorial plasma depletion.

EPDs correspond to the large-scale structure (few tens to hundreds of kilometers) of topside spread  $F$ . They are characterized by steep plasma density gradients that strongly affect radio wave propagation, causing outages and degradation of satellite signals (see Woodman, 2009).

In this study, we concentrate on the balance between magnetic and plasma pressure across strong plasma density gradients in the equatorial ionosphere. Specifically, we analyze EPDs using simultaneous measurements of the magnetic field and electron density from the European Space Agency's Swarm constellation mission. Apart from a spatial and temporal assessment of about 5 years of events, this paper presents the first observational evidence of high plasma pressure in regions of reduced plasma density in the ionosphere.

## 2. Background

EPDs occur in the postsunset ionosphere as depleted wedge-like structures or depleted flux tubes aligned with the ambient magnetic field (see Figure 1a). The EPDs are believed to extend in latitude between magnetic conjugate points in the Northern and Southern Hemispheres and altitude from the bottom side  $F$  region up to about 2,000 km (see Hysell, 2000). The EPD-related current system comprises ambipolar, diamagnetic, and field-aligned currents closing through zonal currents (e.g., Aveiro et al., 2011; Bhattacharyya & Burke, 2000; Dao et al., 2013). Both field-aligned and diamagnetic currents are regularly detected by high-precision magnetometers on board LEO satellites such as CHAMP and Swarm (e.g., Lühr et al., 2002; Rodríguez-Zuluaga & Stolle, 2019; Stolle et al., 2006).

In the ionosphere, as in all magnetized plasmas, there is a drift exclusively related to plasma pressure gradients. This drift is commonly referred to as diamagnetic drift ( $\mathbf{V}_d$ ) and is perpendicular to both the ambient magnetic field and the plasma pressure gradient, as described by

$$\mathbf{V}_{d,j} = -\frac{\nabla p_j \times \mathbf{B}}{q_j n_j B^2}, \quad (1)$$

where  $p_j = n_j k T_j$  is the partial plasma pressure,  $n$  is the number density,  $k$  is the Boltzmann constant,  $T$  is the temperature,  $\mathbf{B}$  is the ambient magnetic field, and  $q$  is the charge of the particle. The subscript  $j$  refers to either electrons  $e$  or ions  $i$ . Figure 1a shows a wedge-like EPD and a Swarm satellite crossing through. Figure 1b depicts a zonal cross section at the dip equator of the EPD in Figure 1a, as seen from the Southern Hemisphere. The box on the right shows a zoom in to the ions gyrating in the magnetic field. This particular example considers an isothermal condition, meaning the gyration radii of the particles inside and outside the EPD are the same. As illustrated in the diagram, the higher-density region rules the direction of the total net drift at the edges of the EPD.

Since electrons and ions drift in opposite directions, as denoted by  $q$  in equation (1), a current  $\mathbf{j}_d$  is built up as shown in Figures 1a and 1b (thick black lines) and described by

$$\mathbf{j}_d = q_e (n_i \mathbf{V}_{d,i} - n_e \mathbf{V}_{d,e}) = -\frac{\nabla p \times \mathbf{B}}{B^2}; \quad p = p_i + p_e. \quad (2)$$

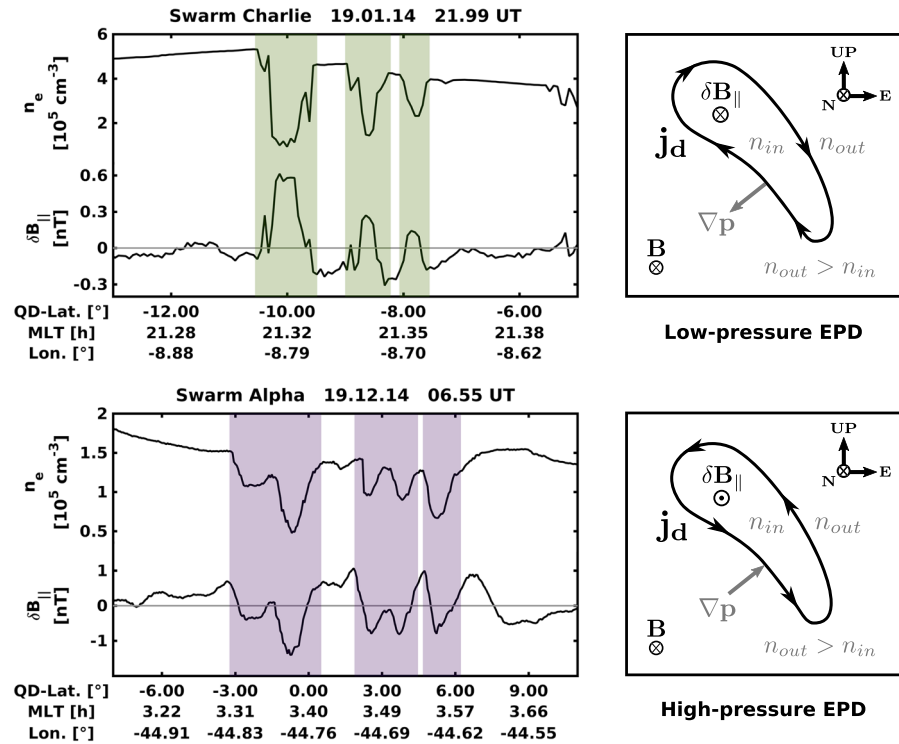


**Figure 2.** (left column) Passes of Swarm Charlie (top) and Alpha (bottom) at equatorial latitudes showing electron density  $n_e$  and  $\delta B_{\parallel}$  as a function of quasi-dipole latitude, magnetic local time, and longitude. (right column) Diagrams describe the plasma pressure gradient  $\nabla p$ , the current  $\mathbf{j}_d$ , and its related magnetic field  $\delta \mathbf{B}_{\parallel}$  for each observation. MLT = magnetic local time; EPD = equatorial plasma depletion.

The current  $\mathbf{j}_d$  is generally known as diamagnetic current since its associated magnetic field opposes the ambient magnetic field in the region where the plasma pressure enhances. Since  $\mathbf{j}_d$  is perpendicular to both  $\mathbf{B}$  and  $\nabla p$ , its related magnetic perturbation is parallel to the ambient field ( $\delta \mathbf{B}_{\parallel}$ , positive northward). A relation for such magnetic effect is described by Lühr et al. (2003) for a steady state plasma as

$$\delta B_{\parallel} = -\delta n_e k(T_e + T_i) \frac{\mu_0}{B}. \quad (3)$$

Here  $\mu_0$  is the permeability of free space, and  $\delta n_e$  is the difference between the electron density outside and inside the EPD ( $\delta n_e = n_{\text{out}} - n_{\text{in}}$ ). The negative sign indicates the decrease of the ambient magnetic field when the plasma pressure increases. In this relation, the balance between magnetic and plasma pressure occurs under isothermal conditions and when the plasma pressure gradient is positive (pointing outside the EPD). The neglect of the magnetic tension due to the curvature of the magnetic field lines is justified for structures much smaller than the bending radius of the ambient field lines.

### 3. Observations

The Swarm mission consists of three satellites (Alpha, Charlie, and Bravo) flying in near-polar circular orbits. The first two satellites fly side by side at an altitude of about 450 km separated by  $1.4^\circ$  in longitude at the equator, while Bravo orbits at a higher elevation of about 510 km. This study uses Swarm magnetic field and electron density measurements at a rate of 1 and 2 Hz, respectively. The latter are decimated to 1 Hz to match the former. A detailed description of the payloads on board Swarm is given by Knudsen et al. (2017) and Tøffner-Clausen et al. (2016).

The method for detection of EPDs is described by Rodríguez-Zuluaga and Stolle (2019). To assess the balance between the plasma and magnetic pressure, we only consider EPDs with a good linear correlation between  $\delta B_{\parallel}$  and  $\delta n_e$ . That is, the absolute value of the correlation coefficients ( $|cc|$ ) must be greater than or equal to 0.6. Figure 2 presents two typical cases of detected EPDs. In the first case (top left panel), a pass of Swarm Charlie shows EPDs with  $\delta B_{\parallel}$  in antiphase with  $\delta n_e$ . In the second case (bottom left panel), a crossing of

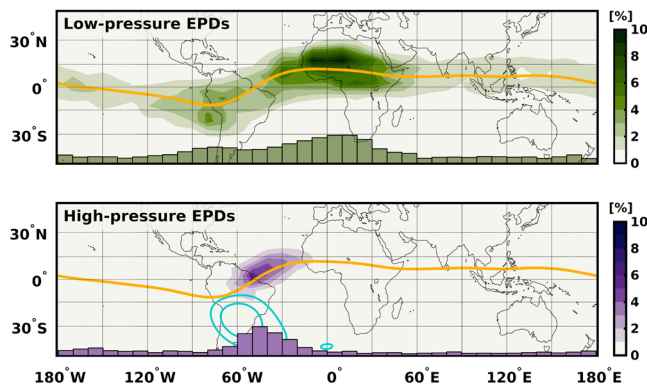


**Figure 3.** Occurrence rate of low-pressure EPDs (top) and high-pressure EPDs (bottom) in a grid of  $10^\circ \times 5^\circ$  in longitude and latitude, respectively. The longitudinal variation of the occurrence rate is depicted qualitatively by histograms at the bottom of each panel ( $10^\circ$  bin). The highest value of events in each histogram is 665 (green) and 305 (purple). The yellow line represents the dip equator. The blue lines in the bottom panel depict the intensity of the magnetic field at the South Atlantic magnetic anomaly. The inner and outer contours correspond to 23,000 and 24,000 nT, respectively. EPD = equatorial plasma depletion.

Swarm Alpha shows EPDs with  $\delta B_{\parallel}$  in phase with  $\delta n_e$ . From the sign of  $\delta B_{\parallel}$  (positive in the direction of  $\mathbf{B}$ ), we can infer the orientation of both  $\mathbf{j}_d$  and  $\nabla p$  as equation (2) suggests. The two current and pressure configurations are depicted on the right panels of Figure 2 using the diagram described in Figure 1b. For the EPDs on the top left panel, the graph on the top right shows a positive  $\delta B_{\parallel}$  related to a clockwise  $\mathbf{j}_d$  and a positive  $\nabla p$  (pointing outside the EPD). For the EPDs on the bottom left panel, the graph on the bottom right shows a negative  $\delta B_{\parallel}$  related to an anticlockwise  $\mathbf{j}_d$  and a negative  $\nabla p$  (pointing inside the EPD). Based on the plasma pressure gradient suggested by the configuration of the diamagnetic currents, these two types of EPDs are referred to as low- and high-pressure EPDs, respectively.

The forthcoming statistical analysis uses simultaneous observations of the magnetic field and electron density obtained from the three Swarm satellites, starting in December 2013 until April 2018. Among the total number of EPDs detected, 81.7% correspond to low-pressure EPDs, while 18.3% to high-pressure EPDs. Figure 3 shows the occurrence rate of both types of EPDs. The occurrence rate considers the total number of passes of each satellite between 18 and 6 LT. It shows that low-pressure EPDs occur at all longitudes while, high-pressure EPDs concentrate mainly over the South American/Atlantic region, between about  $70^\circ\text{W}$  and  $10^\circ\text{W}$  (54% of

the total number of high-pressure EPDs). The histogram at the bottom of each map is meant to describe the longitudinal variability of the occurrence of EPDs only. The values are scaled for each panel with maxima of 665 and 305 for low- and high-pressure EPDs, respectively. Among the total number of EPDs detected between  $70^\circ\text{W}$  and  $10^\circ\text{W}$ , 67.1% correspond to low-pressure EPDs and 32.9% to high-pressure EPDs. It is interesting to note that low-pressure EPDs are detected mainly “off” the equator (by about  $10^\circ$  in latitude), while high-pressure EPDs are detected near the equator. It may result from the fact that high-pressure EPDs mostly occur in a region of lower apex height, as it is shown later in the paper.

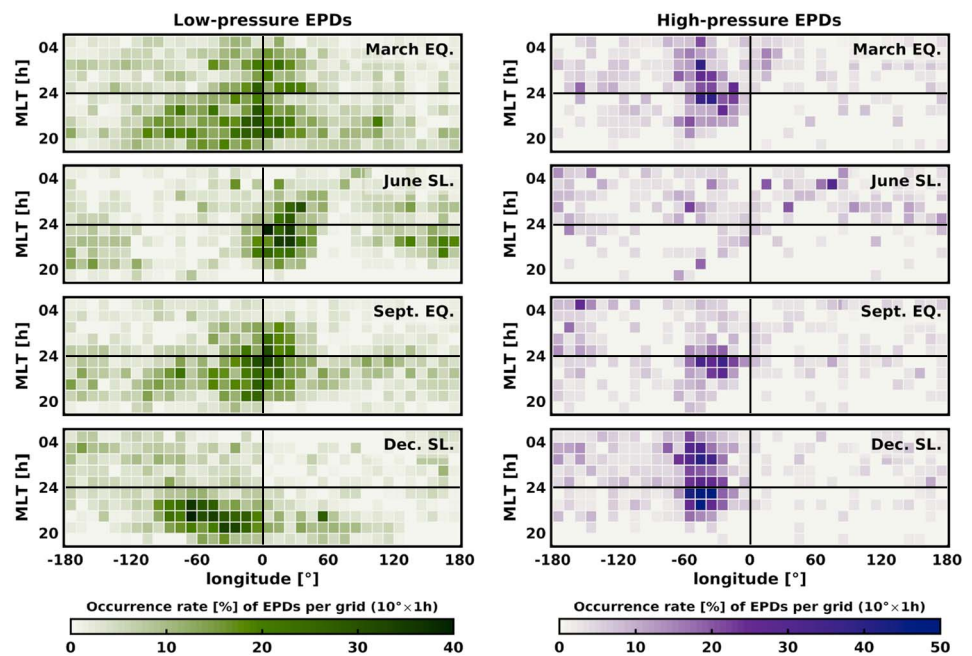


**Figure 4.** Occurrence rate of low-pressure EPDs (left column) and high-pressure EPDs (right column) as a function of magnetic local time and longitude. Each panel from top to bottom corresponds to March equinox, June solstice, September equinox, and December solstice. EPD = equatorial plasma depletion.



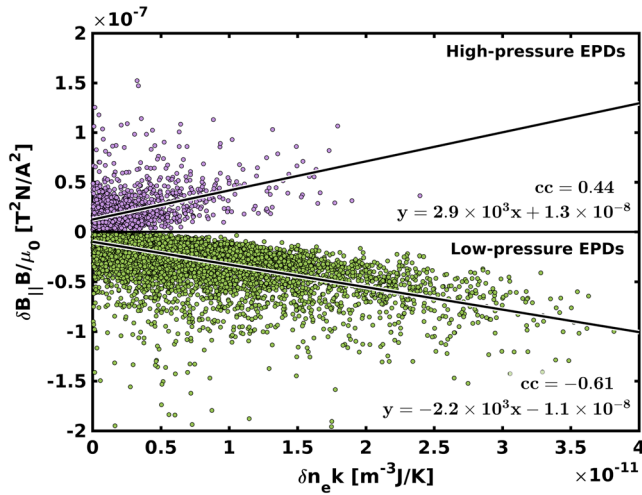


**Figure 5.** Linear regression between the magnetic pressure and electron density variations for all the EPDs detected. Green dots represent low-pressure EPDs, and purple dots high-pressure EPDs. In black are regression lines, related equations, and correlation coefficients. EPD = equatorial plasma depletion.

pressure) depends on the orientation of the magnetic perturbation  $\delta B_{\parallel}$  related to the diamagnetic current. As already specified, all the events in this study correspond to EPDs with good correlation between  $\delta B_{\parallel}$  and  $\delta n_e$  (i.e.,  $|cc| \geq 0.6$ ).

By assuming a pressure balance between an EPD and the ambient plasma, we can estimate the mean temperature, that is,  $(T_{in} + T_{out})/2$ , from the correlation between  $\delta B_{\parallel} B / \mu_0$  and  $\delta n_e k$  as equation (3) suggests. Figure 5 presents such linear regression for both low-pressure EPDs (green dots) and high-pressure EPDs (purple dots). It shows that high-pressure EPDs have mostly low values of  $\delta n_e k$  ( $< 2 \text{ m}^{-3}\text{J/K}$ ) which implies they are shallow EPDs. The different distribution for the two types of EPDs in the regression is expected. It indicates, as is also observed in Figure 2, that  $\delta B_{\parallel}$  and  $\delta n_e$  are inversely and directly proportional across low- and high-pressure EPDs, respectively. At first sight, the values of  $\delta B_{\parallel} B / \mu_0$  and  $\delta n_e k$  for both types of EPDs seem to follow a linear trend among the events. The better correlation for low-pressure EPDs ( $-0.61$ ) might suggest that the balance between magnetic and plasma pressure comes mainly from variations of the plasma density. In other words, changes in the temperature across low-pressure EPDs appear not to play a significant role in the pressure balance. Another possible evidence of this stands on the mean temperature deduced from the slope of the linear regression. The value of 2200 K is quite close to the expected ambient plasma temperature of about 2000 K during premidnight hours (e.g., Lühr et al., 2003) and could confirm on average the assumption of isothermal conditions across of low-pressure EPDs. In the case of high-pressure EPDs, the low value of the correlation (0.44) might suggest that an additional parameter to plasma density, probably the temperature, plays a significant role in the pressure balance. A reasonable indication of this could be the value of the mean temperature (2900 K) deduced from the slope of the regression. It implies that high-pressure EPDs exhibit on average higher temperatures relative to the ambient plasma temperature, if the latter is assumed to be about 2000 K, as previously mentioned.

By defining the plasma pressure gradient as

$$\nabla p = \nabla(nkT) = k(T\nabla n + n\nabla T), \quad (4)$$

we can infer the magnitude of the temperature necessary for EPDs to present low- or high-plasma pressure. For low-pressure EPDs ( $\nabla p > 0$ , pointing outside the EPD), there are three cases: (1) The temperature inside an EPD is the same as outside ( $T_{in} = T_{out}$ , isothermal). (2) The temperature inside an EPD is lower than outside ( $T_{in} < T_{out}$ ). (3) The temperature inside an EPD is higher than outside ( $T_{in} > T_{out}$ ) and  $|T\nabla n| > |n\nabla T|$ . On the other side, high-pressure EPDs ( $\nabla p < 0$ , pointing inside the EPD) can only occur when the temperature inside an EPD is higher than outside and  $|T\nabla n| < |n\nabla T|$ . An estimation for the

Figure 4 shows two columns of four panels each. From left to right, the columns correspond to low- and high-pressure EPDs. Each panel depicts the occurrence rate as a function of magnetic local time (MLT) and longitude for March equinox (February, March, April), June solstice (May, June, July), September equinox (August, September, October), and December solstice (November, December, January). Overall, low-pressure EPDs occur at all local times, except during December solstice where they have a preference for premidnight hours. High-pressure EPDs dominate around midnight and postmidnight hours with an earlier occurrence during December solstice. In general, the seasonal distribution of both low- and high-pressure EPDs agrees with the occurrence rate of EPDs known from earlier studies (e.g., Xiong et al., 2010, and references therein). It is interesting to note that the longitudinal distribution of the low-pressure EPDs varies with the seasons but not that of the high-pressure EPDs, which mostly occur between about  $70^\circ\text{W}$  and  $10^\circ\text{W}$ .

#### 4. Discussion

As previously mentioned, the current driven by a plasma pressure gradient flows in such a way that it decreases/enhances the magnetic field in the region of highest/lowest plasma pressure (see Figure 2). In this study, the criterion to define EPDs as low- or high-pressure EPDs (i.e., plasma

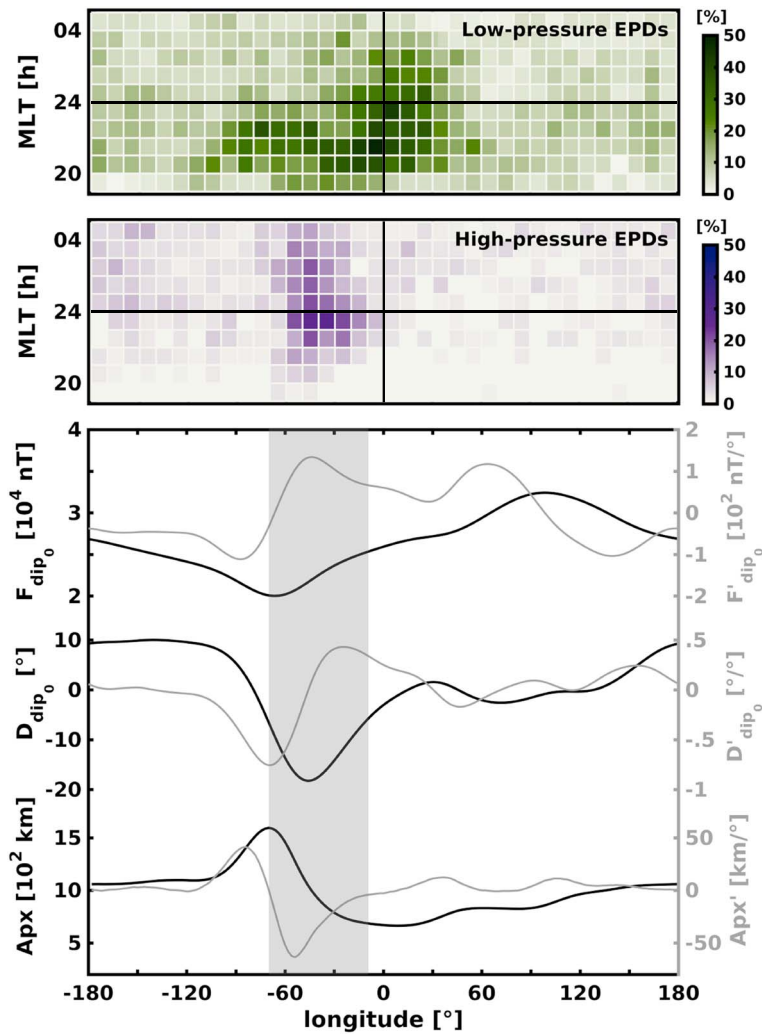


**Figure 6.** Occurrence rate of all (first panel) low-pressure EPDs (green) and (second panel) high-pressure EPDs (purple) as a function of magnetic local time and longitude. (third panel) From top to bottom, magnetic field intensity ( $F$ ) and declination ( $D$ ) at the dip equator, and magnetic field apex height ( $A_{\text{px}}$ ) for field lines within  $\pm 40^\circ$  of magnetic inclination. Gray lines show the first derivative of each parameter as a function of longitude. EPD = equatorial plasma depletion.

temperature inside a high-pressure EPD with respect to the temperature of the ambient plasma comes from equation (4) as

$$T_{\text{in}} > \frac{n_{\text{out}}}{n_{\text{in}}} T_{\text{out}}. \quad (5)$$

By taking measurements of the background density ( $n_{\text{out}}$ ) and minimum density inside the depletions ( $n_{\text{in}}$ ), we calculate the ratio  $n_{\text{out}}/n_{\text{in}}$  for each high-pressure EPD. The result shows a median of 1.96 (95% bootstrap confidence interval of 1.92–2.00) which suggests that for an EPD to present high-plasma pressure,  $T_{\text{in}}$  must be roughly twice  $T_{\text{out}}$  or higher.

It is known from numerical simulations and observations that the plasma temperature within EPDs can be lower or higher than the background. Using the SAMI3/ESF code, Huba et al. (2009) show that EPDs undergo both cooling and heating during their evolution. The authors suggest that the cooling is due to the increase of the EPD volume while rising, and the heating to the compression of ions when streaming down to the EPD feet, where magnetic field lines converge. Such a heating process has also been suggested by Park, Min, et al. (2008) using observations from the ROCSAT-1, KOMPSAT-1, and DMSP missions. The authors describe that EPDs with enhanced temperatures are mainly related to fast poleward field-aligned

flows relative to the ambient plasma (about 260 m/s). In another study, Oyama et al. (1988) propose two additional heating sources of EPDs, one by photoelectrons and another by particle precipitation. These two cases are based on electron temperature measurements across EPDs from the Japanese satellite Hinotori. In the first case, the authors found EPDs with temperatures as high as twice the background temperature between 4 and 9 LT. Due to the early hours, they associate the heating to the interaction with photoelectrons. In the second case, the authors found EPDs with enhanced temperatures of about 300 K relative to the background between 22 and 4 LT and located mainly over the South Atlantic magnetic anomaly (SAA). Because of the specific location, they relate the heating to particle precipitation.

The Swarm mission provides electron temperature measurements gathered by the Langmuir probes. Lomidze et al. (2018) validated the temperature with measurements of ground-based radars. The authors found that temperatures measured by Swarm usually overestimate by 300–400 K those measured by radars. However, the comparison between the two measurements presents high correlations (0.92–0.97) against the validation data. Even so, by looking at the temperature measurements, we note that suspicious fluctuations appear in regions of strong plasma density gradients, such as across EPDs. The electron temperatures from the Langmuir probes are derived assuming that the electrons have a Maxwellian velocity distribution in a coordinate system fixed with respect to the probe (Abe & Oyama, 2013). In the case of a high-energy population associated with high-pressure EPDs, the temperature measurements could be inaccurate since particle distribution significantly deviates from a Maxwellian. Consequently, we prefer not to present any electron temperature measurement in this study.

The characteristics of the magnetic field at equatorial magnetic latitudes can also be of great importance to understand our observations. Figure 6 presents three panels. The first and second panels show the occurrence rate of all detected low- and high-pressure EPDs as a function of magnetic local time (MLT) and longitude. From top to bottom, the third panel depicts the intensity ( $F$ ) and declination ( $D$ ) of the magnetic field at the dip equator, and the apex height (Apx), as well as their first derivatives as a function of longitude. The apex height is for magnetic field lines within  $\pm 40^\circ$  of inclination. This interval corresponds to a rough estimation of the region where EPDs generally occur. Based on LEO satellite data, earlier studies have shown that the occurrence rate of EPDs takes place within about  $\pm 30^\circ$  of magnetic latitude, with the highest occurrence at about  $\pm 10^\circ$  (e.g., Stolle et al., 2006; Xiong et al., 2010). The region shaded in gray in the third panel of Figure 6 highlights the interval with the highest variations of the ambient magnetic field (see gray lines). In this region, the magnetic field intensity at the dip equator increases eastward from its minimum at about  $70^\circ\text{W}$ . Due to such increase of  $F$ , a sharp decrease of the apex height occurs from its maximum of about 1,700 km at  $70^\circ\text{W}$  to a minimum of about 700 km at  $10^\circ\text{W}$ . Another exciting feature is the highest magnetic declination of about  $-20^\circ$  at  $45^\circ\text{W}$ . The particular magnetic configuration of this region might influence different processes in the ionosphere that affect the evolution of EPDs. For example, what can happen to EPDs that grow and drift zonally to a region of higher magnetic intensity (lower apex height)? This is the case for EPDs in the region where high-pressure EPDs are mostly detected (see Figure 6,  $70^\circ\text{--}10^\circ\text{W}$ ). If we assume an EPD originates around  $70^\circ\text{W}$  at about 18 MLT and drifts zonally eastward at 150 m/s (e.g., Makela et al., 2005), it should reach  $45^\circ\text{W}$  at about 23 MLT. This latter longitude and MLT agree with those of the highest occurrence rate of high-pressure EPDs. At first glance, we might expect these EPDs undergo compression while drifting as the magnetic pressure increases with longitude. In that regard, we can roughly estimate the rise in temperature by calculating the volume change of a magnetic flux tube from  $70^\circ\text{W}$  to  $45^\circ\text{W}$ . Assuming an isotropic ionosphere, the temperature rises by only 8.6%, corresponding to a decrease of the magnetic flux tube volume by 11.8%. If indeed heating by adiabatic compression may contribute to the rise of temperature within EPDs in this region, it would not be sufficient for reaching temperatures as high as twice the ambient plasma temperature, as the result from equation (5) suggests. On the other side, there is an additional phenomenon that might help in raising the temperature within EPDs. Due also to the characteristics of the ambient magnetic field in this region and its vicinities (i.e., the SAA), particle precipitation could be a more effective heating mechanism within EPDs, as proposed by Oyama et al. (1988). In their study, the authors conclude that in such a case, the heating of plasma inside EPDs can only occur by the interaction of thermal electrons with fast electrons (soft electrons) flowing along magnetic field lines. Since most of the high-pressure EPDs are shallow (see Figure 5,  $\delta n_e k < 2 \text{ m}^{-3} \text{ J/K}$ ), the heating process should not require that much energy to achieve temperatures within EPDs as high as the double of the background. Therefore, it is likely that low-pressure EPDs generated at  $70^\circ\text{W}$  get heated while crossing SAA longitudes and reach the temperature necessary to become high-pressure EPDs at about  $45^\circ\text{W}$  (see Figure 3, bottom panel). Certainly,



this suggestion must be tested in a further study by using measurements of electron fluxes and if possible of electron temperatures across EPDs. In this paper, we consider only magnetic and plasma pressures and neglect other contributions to the pressure balance, such as plasma inertia and ion/neutral friction. In this respect, the use of measurements of the electric field across EPDs might also help us to better understand the pressure balance mechanism, especially in the case of high-pressure EPDs.

## 5. Summary and Conclusions

In this study, we report the first observational evidence of high plasma pressure in depleted density regions in the ionosphere. The detected structures correspond to large-scale EPDs with a decrease of the magnetic field within the EPD. To assess the balance between magnetic and plasma pressures across both low- and high-pressure EPDs, continuous magnetic field and electron density measurements from the Swarm constellation mission are used from December 2013 to April 2018. The criterion to define an EPD as of low or high pressure (plasma pressure) is the orientation of its related diamagnetic current. The main results and conclusions of this study are as follows:

1. For low-pressure EPDs, the plasma pressure gradient is mostly dominated by variations of the plasma density. Changes in the plasma temperature are not expected to play a significant role. On the contrary, variations of the plasma temperature are significant for high-pressure EPDs.
2. Among all the EPDs detected, 18.3% correspond to high-pressure EPDs and 81.7% to low-pressure EPDs.
3. High-pressure EPDs occur at the American/Atlantic sector mainly, between about 70°W and 10°W, corresponding to 54% of the total number of high-pressure EPDs detected. A preference in magnetic local time is found around midnight and postmidnight hours.
4. High-pressure EPDs are apparently characterized by temperatures as high as twice the ambient plasma temperature.
5. Based on the location of the highest occurrence rate of high-pressure EPDs (i.e., near the SAA), we suggest the main heating mechanism to be due to particle precipitation from the radiation belts.

## Acknowledgments

The European Space Agency (ESA) is acknowledged for providing the Swarm data, which are accessible via the website (<https://earth.esa.int/swarm>). J. Rodríguez-Zuluaga is supported by the Special Priority Programme (SPP) 1788 “DynamicEarth” of the German Research Foundation (DFG). Y. Yamazaki is supported by the Humboldt Research Fellowship for Experienced Researchers from the Alexander von Humboldt Foundation. J. L. Chau’s participation in this work is part of the project supported by DFG under SPP 1788 “DynamicEarth”—CH 1482/1-1 (DYNAMITE).

## References

- Abe, T., & Oyama, K. I. (2013). Langmuir probe. In K.-I. Oyama, & C. Z. Cheng (Eds.), *An introduction to space instrumentation* (pp. 63–75). Tokyo, Japan: Terrapub. Online at <http://www.terrapub.co.jp/onlineproceedings/ste/aisi/index.html>
- Alken, P., Maute, A., & Richmond, A. (2017). The *F*-region gravity and pressure gradient current systems: A review. *Space Science Reviews*, 206(1–4), 451–469.
- Aveiro, H., Hysell, D., Park, J., & Lühr, H. (2011). Equatorial spread *F*-related currents: Three-dimensional simulations and observations. *Geophysical Research Letters*, 38, L21103. <https://doi.org/10.1029/2011GL049586>
- Bhattacharyya, A., & Burke, W. J. (2000). A transmission line analogy for the development of equatorial ionospheric bubbles. *Journal of Geophysical Research*, 105(A11), 24,941–24,950.
- Dao, E., Seyler, C., & Kelley, M. (2013). Three-dimensional modeling of the electromagnetic characteristics of equatorial plasma depletions. *Journal of Geophysical Research: Space Physics*, 118, 3505–3514. <https://doi.org/10.1002/jgra.50216>
- Forbes, J. M., & Garrett, H. B. (1979). Solar tidal wind structures and the *E*-region dynamo. *Journal of geomagnetism and geoelectricity*, 31(3), 173–182.
- Huba, J., Joyce, G., Krall, J., & Fedder, J. (2009). Ion and electron temperature evolution during equatorial spread *F*. *Geophysical Research Letters*, 36, L15102. <https://doi.org/10.1029/2009GL038872>
- Hysell, D. (2000). An overview and synthesis of plasma irregularities in equatorial spread *F*. *Journal of Atmospheric and Solar-Terrestrial Physics*, 62(12), 1037–1056.
- Knudsen, D., Burchill, J., Buchert, S., Eriksson, A., Gill, R., Wahlund, J. E., & Moffat, B. (2017). Thermal ion imagers and Langmuir probes in the Swarm electric field instruments. *Journal of Geophysical Research: Space Physics*, 122, 2655–2673. <https://doi.org/10.1002/2016JA022571>
- Lomidze, L., Knudsen, D. J., Burchill, J., Kouznetsov, A., & Buchert, S. C. (2018). Calibration and validation of swarm plasma densities and electron temperatures using ground-based radars and satellite radio occultation measurements. *Radio Science*, 53, 15–36. <https://doi.org/10.1002/2017RS006415>
- Lühr, H., Maus, S., Rother, M., & Cooke, D. (2002). First in-situ observation of night-time *F* region currents with the CHAMP satellite. *Geophysical research letters*, 29(10), 1489. <https://doi.org/10.1029/2001GL013845>
- Lühr, H., Rother, M., Maus, S., Mai, W., & Cooke, D. (2003). The diamagnetic effect of the equatorial Appleton anomaly: Its characteristics and impact on geomagnetic field modeling. *Geophysical Research Letters*, 30(17), 1906. <https://doi.org/10.1029/2003GL017407>
- Makela, J., Kelley, M., & Su, S. Y. (2005). Simultaneous observations of convective ionospheric storms: ROCSAT-1 and ground-based imagers. *Space Weather*, 3, S12C02. <https://doi.org/10.1029/2005SW000164>
- Oyama, K. I., Schlegel, K., & Watanabe, S. (1988). Temperature structure of plasma bubbles in the low latitude ionosphere around 600 km altitude. *Planetary and space science*, 36(6), 553–567.
- Park, J., Lühr, H., & Min, K. W. (2010). Neutral density depletions associated with equatorial plasma bubbles as observed by the CHAMP satellite. *Journal of Atmospheric and Solar-Terrestrial Physics*, 72(2–3), 157–163.
- Park, J., Min, K. W., Kim, V. P., Kil, H., Su, S. Y., Chao, C. K., & Lee, J. J. (2008). Equatorial plasma bubbles with enhanced ion and electron temperatures. *Journal of Geophysical Research*, 113, A09318. <https://doi.org/10.1029/2008JA013067>

- Park, J., Stolle, C., Lühr, H., Rother, M., Su, S. Y., Min, K. W., & Lee, J. J. (2008). Magnetic signatures and conjugate features of low-latitude plasma blobs as observed by the CHAMP satellite. *Journal of Geophysical Research*, 113, A09313. <https://doi.org/10.1029/2008JA013211>
- Rishbeth, H. (1971). The *F*-layer dynamo. *Planetary and Space Science*, 19, 263–267.
- Rodríguez-Zuluaga, J., & Stolle, C. (2019). Interhemispheric field-aligned currents at the edges of equatorial plasma depletions. *Scientific Reports*, 9(1), 1233.
- Stolle, C., Lühr, H., & Rother, M. (2006). Magnetic signatures of equatorial spread *F* as observed by the CHAMP satellite. *Journal of Geophysical Research*, 111, A02304. <https://doi.org/10.1029/2005JA011184>
- Tøffner-Clausen, L., Lesur, V., Olsen, N., & Finlay, C. C. (2016). In-flight scalar calibration and characterisation of the Swarm magnetometry package. *Earth, Planets and Space*, 68(1), 129.
- Woodman, R. (2009). Spread *F*—An old equatorial aeronomy problem finally resolved? *Annales geophysicae*, 27, 1915–1934. <https://doi.org/10.5194/angeo-27-1915-2009>
- Xiong, C., Park, J., Lühr, H., Stolle, C., & Ma, S. (2010). Comparing plasma bubble occurrence rates at CHAMP and GRACE altitudes during high and low solar activity. *Annales Geophysicae*, 28, 1647–1658. <https://doi.org/10.5194/angeo-28-1647-2010>
- Yokoyama, T., & Stolle, C. (2017). Low and midlatitude ionospheric plasma density irregularities and their effects on geomagnetic field. *Space Science Reviews*, 206(1–4), 495–519.